COPY

OAK RIDGE NATIONAL LABORATORY
OPERATED BY
UNION CARBIDE CORPORATION
NUCLEAR DIVISION
POST OFFICE BOX X
OAK RIDGE, TENNESSEE 37830

ORNL/MIT-283

DATE: December 21, 1978

SUBJECT: Mass Transfer in Three-Phase Fluidized Beds

Authors: F.V. Gay, C.B. Holtman, and N.F. Sheppard

Consultants: J.M. Begovich, S.D. Clinton, and J.S. Watson

ABSTRACT

The effects of superficial gas and liquid velocity and particle diameter on the liquid-side mass-transfer coefficient (K_La) in three-phase fluidized beds were studied using a water-sodium sulfite/air/glass-bead system. A discontinuous-phase sampling system was developed to determine gas-phase concentrations within the bed, and these were used to calculate K_La. Increasing d_p, U_G, and U_L caused an increase in K_La within the region characterized by bubble disintegration. Within the region characterized by bubble coalescence and slug flow, the opposite effect was noted.

MASTER

Oak Ridge Station
School of Chemical Engineering Practice
Massachusetts Institute of Technology
S.M. Senkan, Director

Printed in the United States of America. Available from
National Technical Information Service
U.S. Department of Commerce
5285 Port Royal Road, Springfield, Virginia 22161
Price: Printed Copy $4.50; Microfiche $3.00

Contents

		Page
1.	Summary	5
2.	Introduction	5
	2.1 Background	5
	2.2 Previous Work	6
	2.3 Theory	6
	2.4 Objectives	10
3.	Apparatus and Procedure	10
4.	Results and Discussion	12
	4.1 Mass Transfer Coefficients	12
	4.1.1 Results	12
	4.1.2 Discussion	12
	4.2 Comparison of Two- and Three-Phase $K_L a$'s	20
	4.3 Axial Dispersion Coefficient	22
5.	Conclusions	22
6.	Recommendations	23
7.	Acknowledgments	23
8.	Appendix	24
	8.1 Gas Sampling System	24
	8.2 Sample Calculations	24
	8.3 Summary of Experimental Results	29
	8.4 Nomenclature	31
	8.5 Location of Data	33
	8.6 Literature Cited	33

1. SUMMARY

Mass transfer experiments were conducted in a 7.62-cm-ID cocurrent three-phase fluidized bed using an aqueous sodium sulfite/air/glass bead system. Absorbed oxygen reacting with the sulfite ion resulted in an oxygen-free liquid phase, so that mass transfer was independent of liquid axial dispersion. A discontinuous-phase sampling system was developed to enable gas-phase analysis along the bed. This concentration data were used to calculate mass transfer coefficients within the two- and three-phase regions of the column. Bead diameters of 3.2, 4.6, and 6.2 mm were used at superficial gas velocities of 4.3 to 12.9 cm/s and liquid velocities of 1.28 to 11.2 cm/s.

The three-phase mass-transfer coefficient (K_La) was found to decrease with increasing gas velocity at very high and very low gas velocities; a direct proportionality was found for intermediate velocities. K_La first decreased, then increased with increasing liquid velocity. Increasing the bead diameter caused an increase in the mass transfer coefficient at low gas velocities and a decrease at higher gas velocities. The existence of three regions (bubble coalescence, bubble disintegration, and slugging) are postulated to account for this behavior.

Dispersion coefficients, E_L, were calculated using experimentally determined K_La's and liquid-phase concentration data from earlier studies. The values obtained are nearly zero, suggesting the liquid phase is also in plug flow. Further mass transfer experiments over a wider range of U_L/U_{MF} and U_G are recommended.

2. INTRODUCTION

2.1 Background

Three-phase fluidization in which the solid particles are suspended by upward cocurrent flow of liquid and gas phases is finding increased use in industrial processes because of low cost, high transfer rates, and ease of temperature and residence-time control. The principal application is for gas-liquid reactions which occur on the surface of solid catalysts. Coal liquefaction and gasification, hydrogenation of petroleum fractions and slurry methanation of CO are examples of such processes. Three-phase fluidization also appears attractive for biochemical processes because high mixing rates can be attained with low shear stresses. An understanding of hydrodynamic and mass-transfer behavior in three-phase fluidized beds is essential for the design of such systems. This project is part of a continuing study concerning the behavior of three-phase fluidized beds which began in 1975 by the Chemical Technology Division of ORNL.

2.2 Previous Work

The hydrodynamics of three-phase fluidized beds has been studied extensively (1, 2, 3, 4, 14). Superficial minimum liquid fluidization velocity, $U_{L,MF}$, was found to decrease with increasing superficial gas velocity, U_G, and increase with increasing solids density and diameter, ρ_p and d_p, respectively. Solids holdup decreases with increasing U_G and U_L, but increases with ρ_p. Gas holdup increases with U_G and ρ_p but decreases with U_L. Begovich (1) confirmed the above relationships and also found that solids holdup increases with increasing solids diameter; he also reported a transition region, typically 15% of the bed height, in which solids holdup falls from a constant maximum value to zero. This axial holdup variation was correlated in terms of U_G, U_L, μ_L, σ_{GL}, d_p, ρ_p, D, and H.

Mass transfer has been characterized as functions of U_G, U_L, and d_p (12, 13, 17). K_La was found to increase with U_G but was affected little by changes in U_L. Østergaard (11, 12) presented the concept of a critical particle diameter, below which bubble coalescence characterizes the system and above which bubble disintegration occurs. K_La values for 6-mm beads were found to be ten times those for 1-mm beads, with those for bubble columns having intermediate values. The liquid axial dispersion coefficient was found to increase with U_G, U_L, and d_p (9, 17).

2.3 Theory

The overall mass transfer coefficient, K_La, for gas absorption in a vessel is conventionally related to the liquid-phase concentration profile by a differential mass balance (5, 8):

$$E_L \frac{d^2C_L}{dh^2} - U_L \frac{dC_L}{dh} = K_La(C_G - C_L) \qquad (1)$$

The dispersion coefficient, E_L, measures the backmixing which occurs in the liquid phase. For the gas phase, which can safely be assumed to be in plug flow, dispersion is minimal. Thus,

$$U_G \frac{dC_G}{dh} = - K_La(C_G - C_L) \qquad (2)$$

The overall mass transfer coefficient is related to the gas- and liquid-side coefficients, K_Ga and K_La, by:

$$\frac{1}{K_C a} = \frac{m}{K_G a} + \frac{1}{K_L a} \tag{3}$$

If the Henry's constant, m, is small for the system under consideration, a significant concentration gradient within the gas will not occur (6), and the gas-side resistance will be negligible (12). Therefore,

$$K_C a \doteq K_L a \tag{4}$$

Equations (1) and (2) can now be rewritten:

$$E_L \frac{d^2 C_L}{dh^2} - U_L \frac{dC_L}{dh} = K_L a \, (C_{L,i} - C_L) \tag{5}$$

$$U_G \frac{dC_G}{dh} = -K_L a (C_{L,i} - C_L) \tag{6}$$

Mass transfer coefficients are conventionally determined from the axial concentration profiles, which are obtained by sampling the liquid phase along the column. Values of the dispersion and mass transfer coefficients are then determined simultaneously by matching a theoretical profile to the experimental data. This method is inherently approximate because the mass transfer coefficient is closely related to the dispersion coefficient [see Eq. (5)]. An alternative approach is to measure gas-phase concentrations and use Eq. (6). However, the liquid-phase concentration profile must still be known, necessitating the use of Eq. (5).

A method for determining mass transfer coefficients which avoids these problems is to introduce a liquid-phase chemical reaction. However, the reaction must be slow enough to not influence the rate of absorption from the gas, yet fast enough to react all of the absorbed gas in the bulk liquid (15). The gas-phase mass balance can then be represented by:

$$U_G \frac{dC_G}{dh} = -K_L a \, m C_{G,i} \tag{7}$$

A qualitative oxygen concentration profile is shown in Fig. 1. Two conditions must be met for Eq. (7) to be valid (15). For a reaction which is m^{th} order with respect to the solute gas, A, and n^{th} order with respect to the liquid phase reactant, B, the reaction in the liquid film can be neglected (15) if:

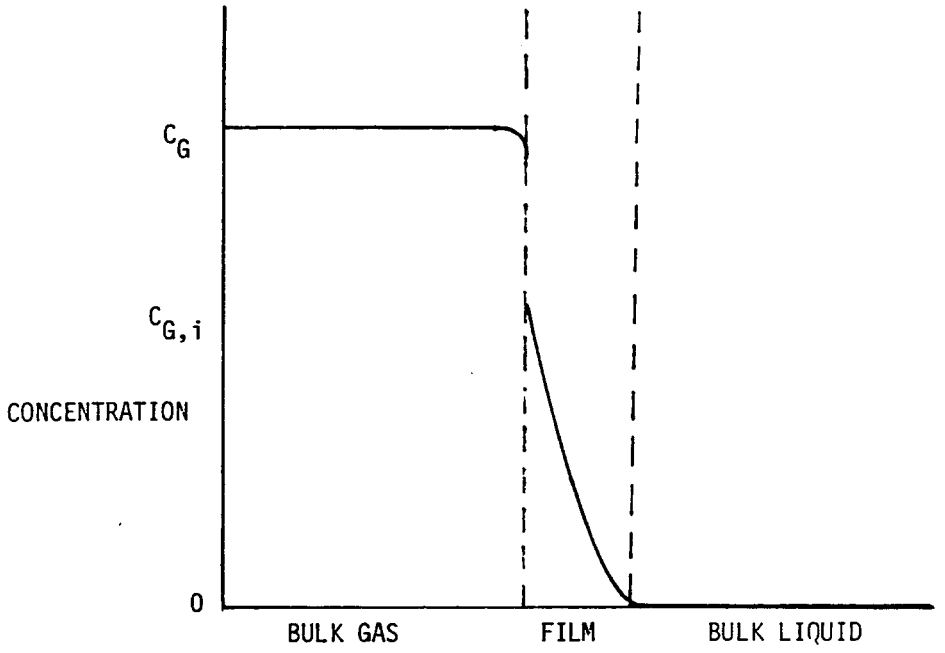

MASSACHUSETTS INSTITUTE OF TECHNOLOGY
SCHOOL OF CHEMICAL ENGINEERING PRACTICE
AT
OAK RIDGE NATIONAL LABORATORY

THEORETICAL O_2 CONCENTRATION PROFILE

DATE	DRAWN BY	FILE NO.	FIG.
12-21-78	CBH	CEPS-X-283	1

$$\frac{(2/n+1)\ D_G\ K_{mn}\ (A)^{m-1}\ (B)^n}{K_L^{\ 2}} << 1 \qquad (8)$$

To assure zero solute gas concentration in the bulk-liquid phase, the following inequality must also hold (15):

$$\frac{K_L a}{\varepsilon_L\ K_{mn}\ (B)^n\ (A)^{m-1}} << 1 \qquad (9)$$

The oxidation of aqueous sodium sulfite was chosen as the reacting system because the reaction rate can be adjusted over a wide range:

$$2\ SO_3^{=} + O_2(aq) \xrightarrow{K_1} 2\ CO_4^{=} \qquad (10)$$

Srivastava (16) reported the reaction to be first order with respect to oxygen, and zero order with respect to sulfite for sulfite concentrations between 0.08 and 0.16 M. The reaction is catalyzed by cobalt and copper ions. The first-order rate-constant ranges for a catalyst-free system from 30 to 300 s^{-1}.

The diffusivity of O_2 in the aqueous sulfite solution is estimated to be 1.96×10^{-5} cm^2/s (5). Østergaard (11) reports K_L values of about 0.06 cm/s for the three-phase fluidization of air/water/glass-beads. The minimum value of the liquid phase dispersion coefficient, E_L, is generally about 0.3, and the maximum $K_L a$ value obtained in this study was about 0.045 s^{-1}.

Substituting these values into inequalities (8) and (9) yields the following constraint on the first-order rate constant K_1:

$$0.15 << K_1 << 184 \qquad (11)$$

Therefore, the use of a catalyst-free system was warranted for the experiments.

The expression for the mass transfer coefficient, in terms of measurable quantitites, can be derived by integrating Eq. (7) along the bed over a region of height Δh which gives:

$$K_L a = \frac{U_G \ln(X_e/X_\ell)}{m \Delta h} \qquad (12)$$

where X_e and X_ℓ are the mole fractions of O_2 in the gas phase entering and leaving the integration region, respectively.

2.4 Objectives

The objectives were: (1) to determine the mass transfer coefficients ($K_L a$) independent of the axial liquid dispersion coefficient (E_L), (2) to study the effects of liquid and gas velocities and particle diameter on $K_L a$, and (3) to verify literature values of E_L from independent $K_L a$ measurements.

3. APPARATUS AND PROCEDURE

The experimental apparatus is illustrated in Fig. 2. Liquid and gas enter through fluid distributors at the bottom of the 7.62-in.-ID column. The inlet gas pressure is measured with a mercury manometer, and additional water manometers are used to determine the column pressure profile. The column is filled with glass beads to a height of 50 cm. Samples can be taken for oxygen analysis from four side ports located 25.5, 49.5, 73.5, and 113.5 cm from the inlet. The method of gas sampling and analysis is described in Appendix 8.1.

Fifty-gallons of a 0.16 M sodium sulfite solution was prepared, using distilled water. The solution was analyzed for possible contamination by copper and cobalt, which catalyze the oxidation reaction (16). Less than 0.2 µg/ml of each ion was present, thus the rate constant was not affected. The sulfite concentration of the liquid was determined iodometrically. This concentration was checked frequently during the experiments, and the solution was discarded when the sulfite concentration reached 0.08 M.

Experimental runs were begun by calibrating the O_2 analyzers, as described in Appendix 8.3. Air and sulfite solution were pumped into the column at controlled rates, and the system was allowed to reach a steady state. Gas-phase oxygen concentrations were measured at the column outlet and at two points within both the three-phase and the two-phase regions. The temperature and barometric and manometric pressures were recorded, and the heights of the three-phase and transition regions were estimated visually. Forty-seven runs were completed, corresponding to the values of the parameters presented in Table 1.

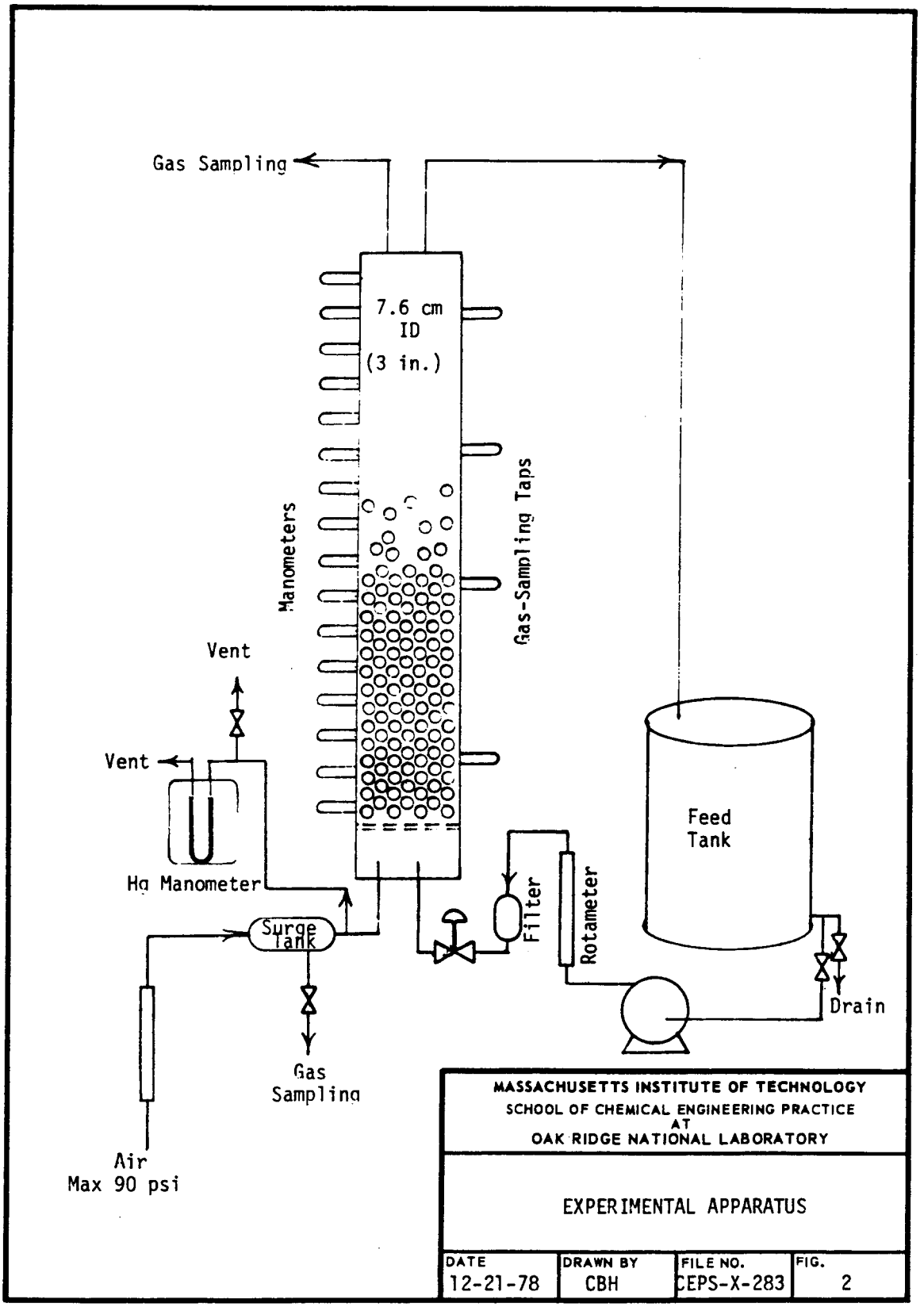
Gas Sampling
7.6 cm
ID
(3 in.)
Manometers
Gas-Sampling Taps
Vent
Vent
Hg Manometer
Surge Tank
Filter
Rotameter
Feed Tank
Drain
Gas Sampling
Air
Max 90 psi
MASSACHUSETTS INSTITUTE OF TECHNOLOGY
SCHOOL OF CHEMICAL ENGINEERING PRACTICE
AT
OAK RIDGE NATIONAL LABORATORY
EXPERIMENTAL APPARATUS
DATE 12-21-78
DRAWN BY CBH
FILE NO. CEPS-X-283
FIG. 2

Table 1. Values of Experimental Parameters

Parameter	Experimental Values			
Superficial Gas Velocity (cm/s)	4.3	8.7	12.9	
Superficial Liquid Velocity*	1.5	2.0	3.0	5.0
Bead Diameter (mm)	3.2	4.6	6.9	

*Relative to $U_{L,MF}$

4. RESULTS AND DISCUSSION

4.1 Mass Transfer Coefficients

4.1.1 Results

The mass transfer coefficients for the three-phase region were calculated by the method outlined in Appendix 8.2.3, and the numerical results appear in Appendix 8.3. In Figs. 3 through 7, K_La's are plotted as functions of U_G, U_L/U_{MF}, and d_p. The uncertainty of each value was determined using the method described in Appendix 8.2.

4.1.2 Discussion

Figures 3 and 4 indicate that K_La varies little with particle diameter for low gas and liquid velocities. The K_La values for the two smaller particles show a steady increase for increasing U_G except for 3.2-mm beads subject to high U_L, for which the K_La first decreases and then increases. This indicates that high U_L causes a coalescing effect, which is overcome at high U_G. As U_L increases, the K_La for 6.0-mm beads shows a more pronounced decrease, which suggests slugging at high gas and liquid velocities.

In Figs. 5 through 7 the K_La values for 3.2- and 4.6-mm beads first decrease and then increase with increasing U_L. This effect appears to be independent of U_G. The K_La values for the 6.0-mm beads increase with increasing U_L at low U_G but exhibit opposite behavior at high U_G. This again indicates slugging.

The system appears to be characterized by three types of behavior as U_G is increased, as indicated in Fig. 8a. At lower U_G, the inertia of the beads is small and coalescence is important. In this region the larger beads greatly enhance transfer. As U_G increases, coalescence is overcome by inertial forces; K_La increases with increasing U_G until slugging becomes significant. At high U_G the gas will appear in the system as slugs; the bubble size will be larger throughout the bed; interfacial area will be reduced and K_La will decrease.

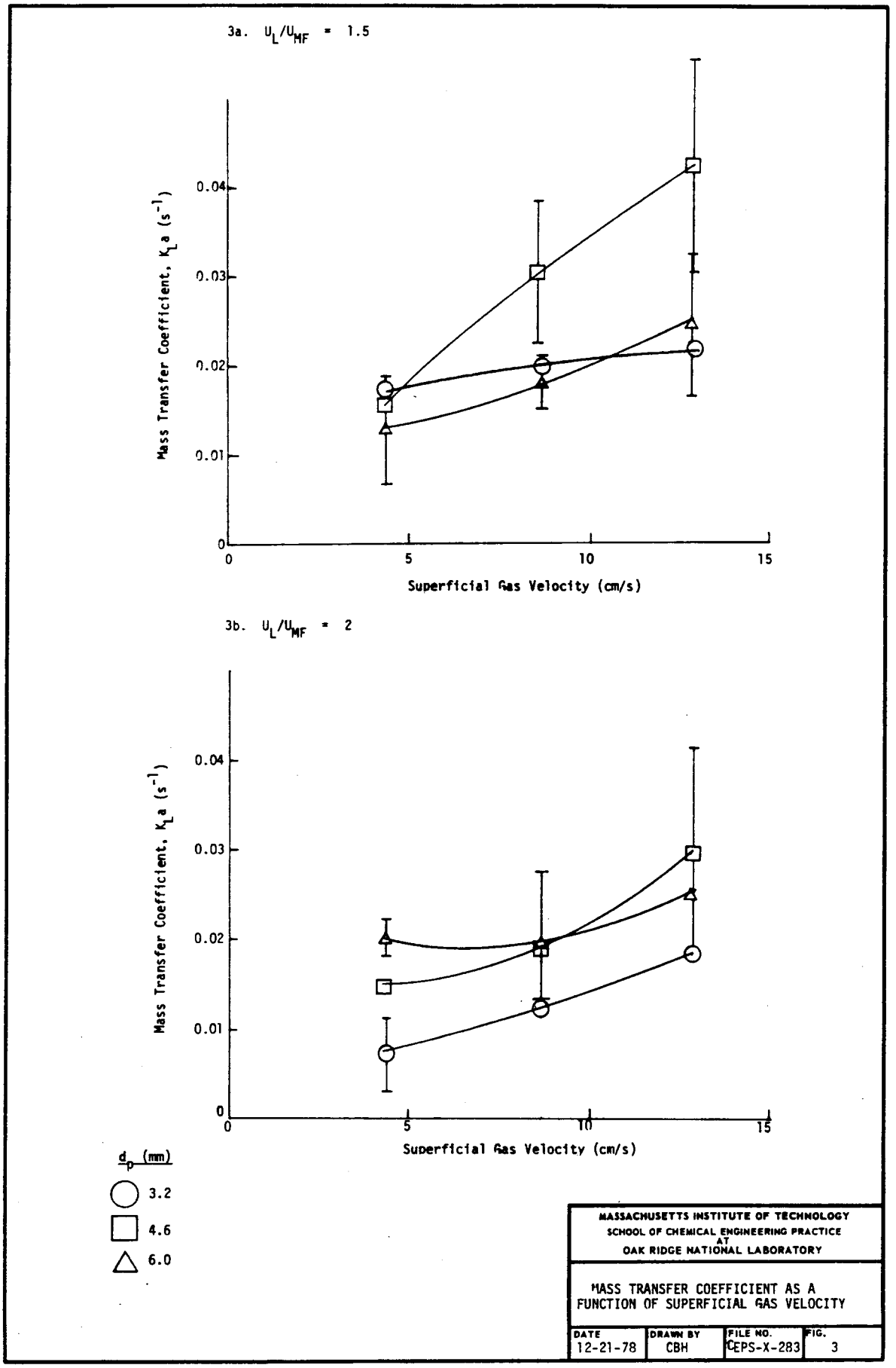
3a. U_L/U_{MF} = 1.5
Mass Transfer Coefficient, K_La (s^{-1})
0.04
0.03
0.02
0.01
0
0
5
10
15
Superficial Gas Velocity (cm/s)
3b. U_L/U_{MF} = 2
Mass Transfer Coefficient, K_La (s^{-1})
0.04
0.03
0.02
0.01
0
0
5
10
15
Superficial Gas Velocity (cm/s)
d_p (mm)
3.2
4.6
6.0
MASSACHUSETTS INSTITUTE OF TECHNOLOGY
SCHOOL OF CHEMICAL ENGINEERING PRACTICE
AT
OAK RIDGE NATIONAL LABORATORY
MASS TRANSFER COEFFICIENT AS A FUNCTION OF SUPERFICIAL GAS VELOCITY
DATE 12-21-78
DRAWN BY CBH
FILE NO. CEPS-X-283
FIG. 3

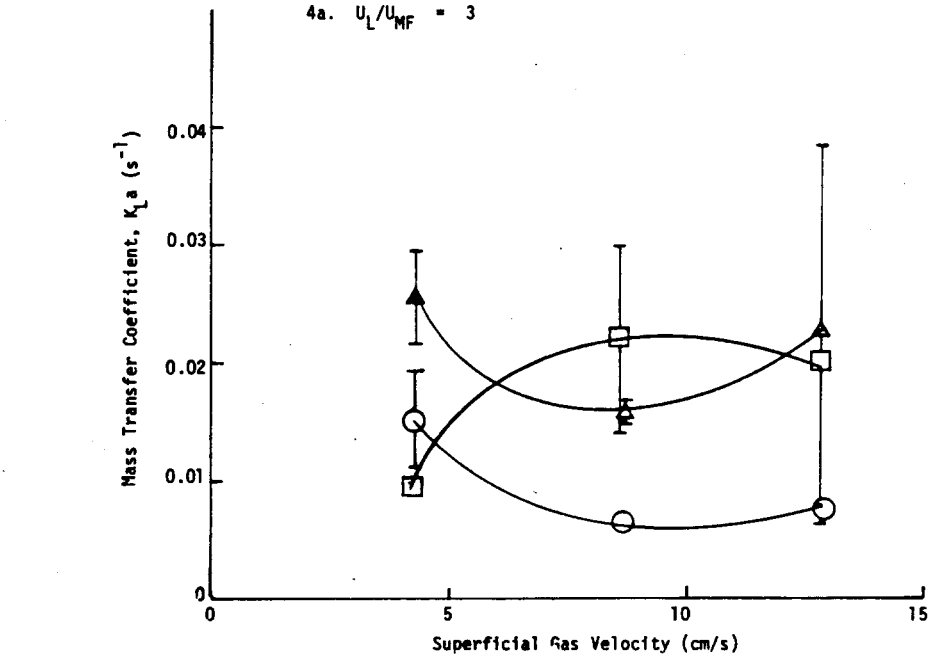

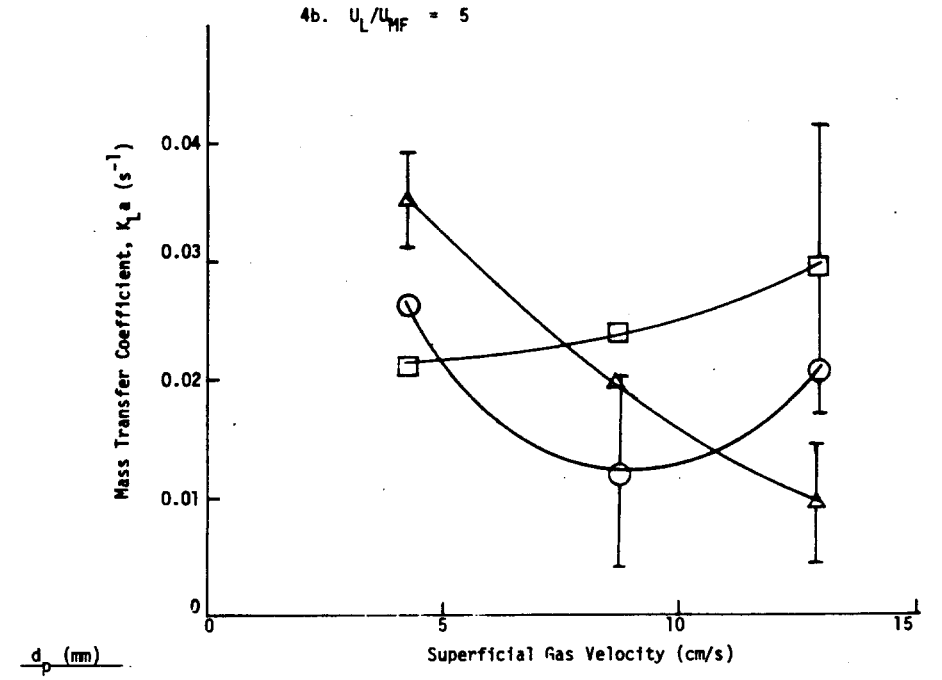

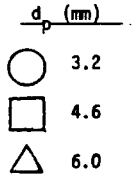

MASSACHUSETTS INSTITUTE OF TECHNOLOGY
SCHOOL OF CHEMICAL ENGINEERING PRACTICE
AT
OAK RIDGE NATIONAL LABORATORY

MASS TRANSFER COEFFICIENT AS A FUNCTION OF SUPERFICIAL GAS VELOCITY

DATE	DRAWN BY	FILE NO.	FIG.
12-21-78	CBH	CEPS-X-283	4

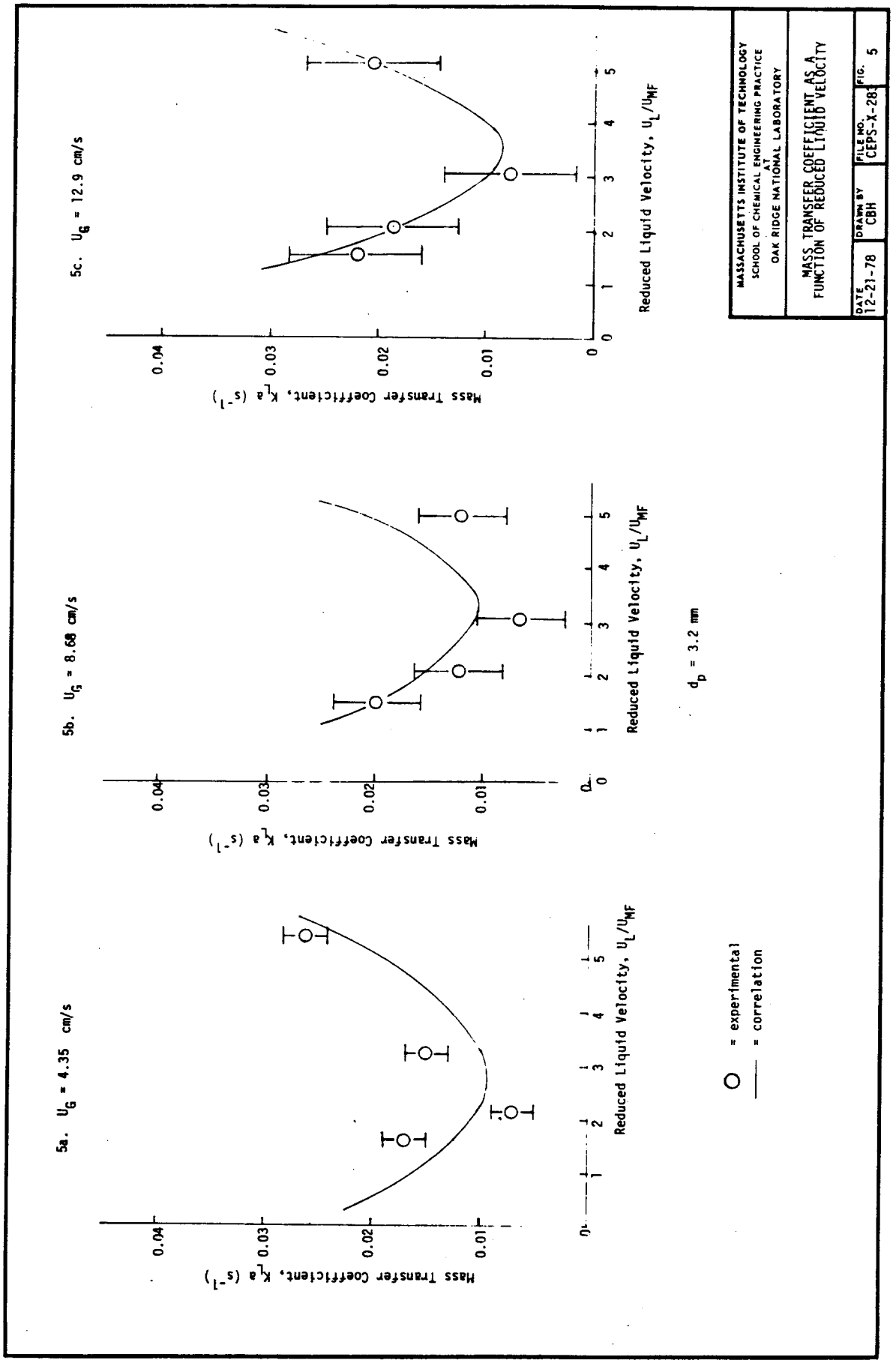
5a. U_G = 4.35 cm/s
5b. U_G = 8.68 cm/s
5c. U_G = 12.9 cm/s
Mass Transfer Coefficient, k_La (s^{-1})
0.04
0.03
0.02
0.01
0
1
2
3
4
5
Reduced Liquid Velocity, U_L/U_{MF}
d_p = 3.2 mm
O = experimental
—— = correlation
MASSACHUSETTS INSTITUTE OF TECHNOLOGY
SCHOOL OF CHEMICAL ENGINEERING PRACTICE
AT
OAK RIDGE NATIONAL LABORATORY
MASS TRANSFER COEFFICIENT AS A FUNCTION OF REDUCED LIQUID VELOCITY
DATE 12-21-78
DRAWN BY CBH
FILE NO. CEPS-X-283
FIG. 5

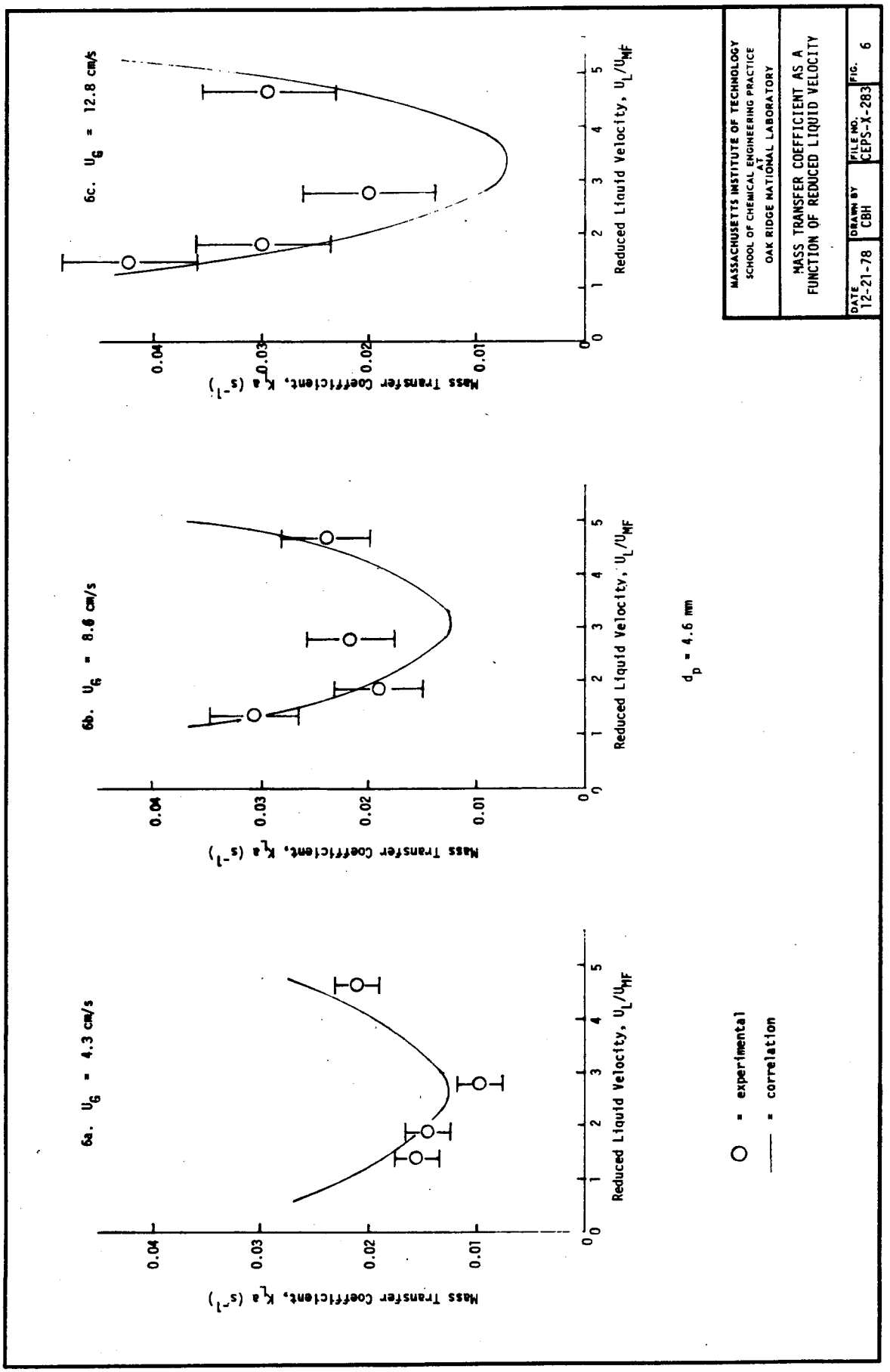
6a. U_G = 4.3 cm/s
6b. U_G = 8.6 cm/s
6c. U_G = 12.8 cm/s
Mass Transfer Coefficient, $K_L a$ (s^{-1})
Reduced Liquid Velocity, U_L/U_{MF}
0.04
0.03
0.02
0.01
0
1
2
3
4
5
d_p = 4.6 mm
O = experimental
—— = correlation
MASSACHUSETTS INSTITUTE OF TECHNOLOGY
SCHOOL OF CHEMICAL ENGINEERING PRACTICE
AT
OAK RIDGE NATIONAL LABORATORY
MASS TRANSFER COEFFICIENT AS A FUNCTION OF REDUCED LIQUID VELOCITY
DATE 12-21-78
DRAWN BY CBH
FILE NO. CEPS-X-283
FIG. 6

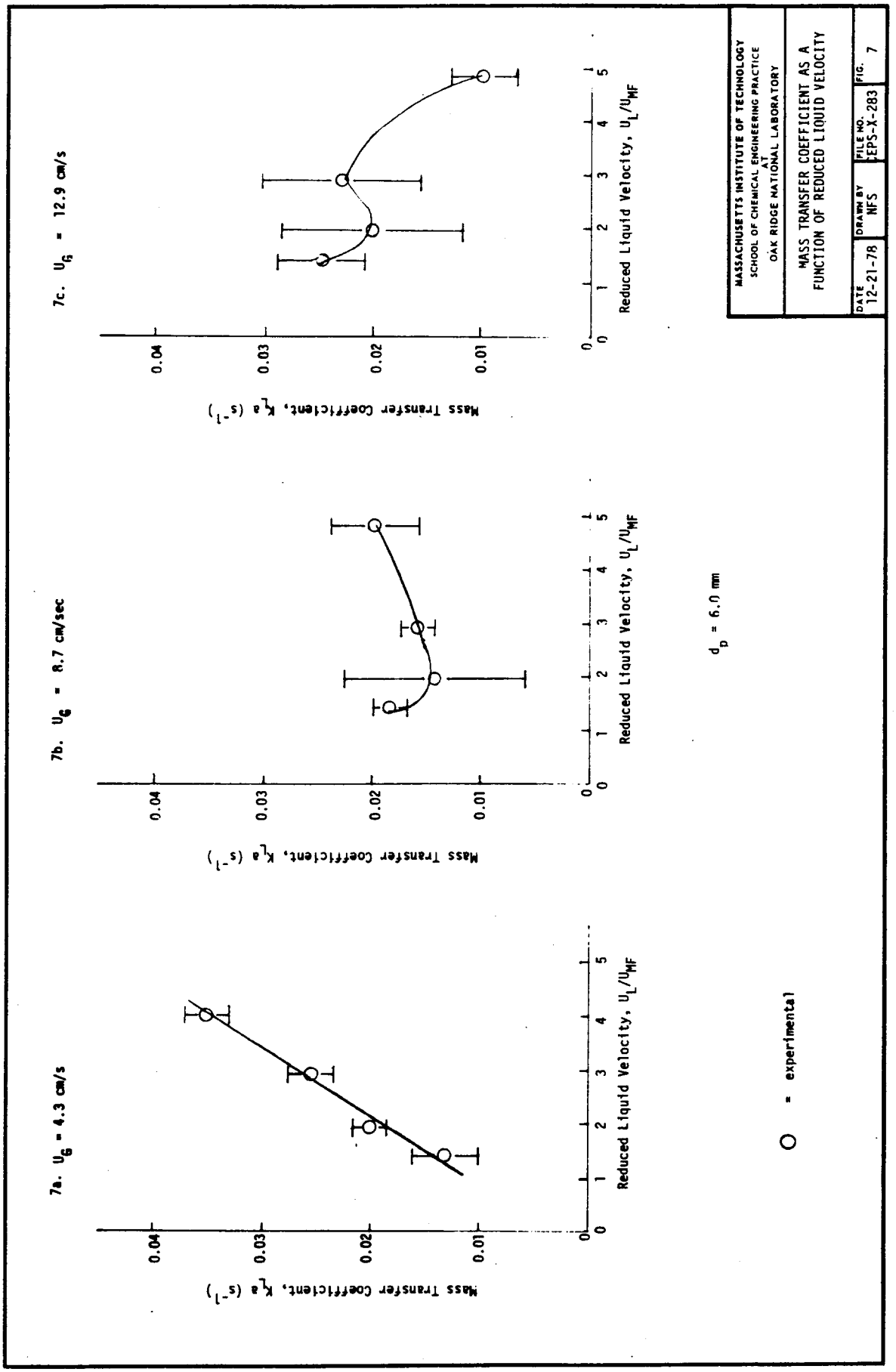
7a. U_G = 4.3 cm/s
7b. U_G = 8.7 cm/sec
7c. U_G = 12.9 cm/s
Mass Transfer Coefficient, K_La (s^{-1})
0.04
0.03
0.02
0.01
Reduced Liquid Velocity, U_L/U_{MF}
0
1
2
3
4
5
O = experimental
d_p = 6.0 mm
MASSACHUSETTS INSTITUTE OF TECHNOLOGY
SCHOOL OF CHEMICAL ENGINEERING PRACTICE
AT
OAK RIDGE NATIONAL LABORATORY
MASS TRANSFER COEFFICIENT AS A FUNCTION OF REDUCED LIQUID VELOCITY
DATE 12-21-78
DRAWN BY NFS
FILE NO. EPS-X-283
FIG. 7

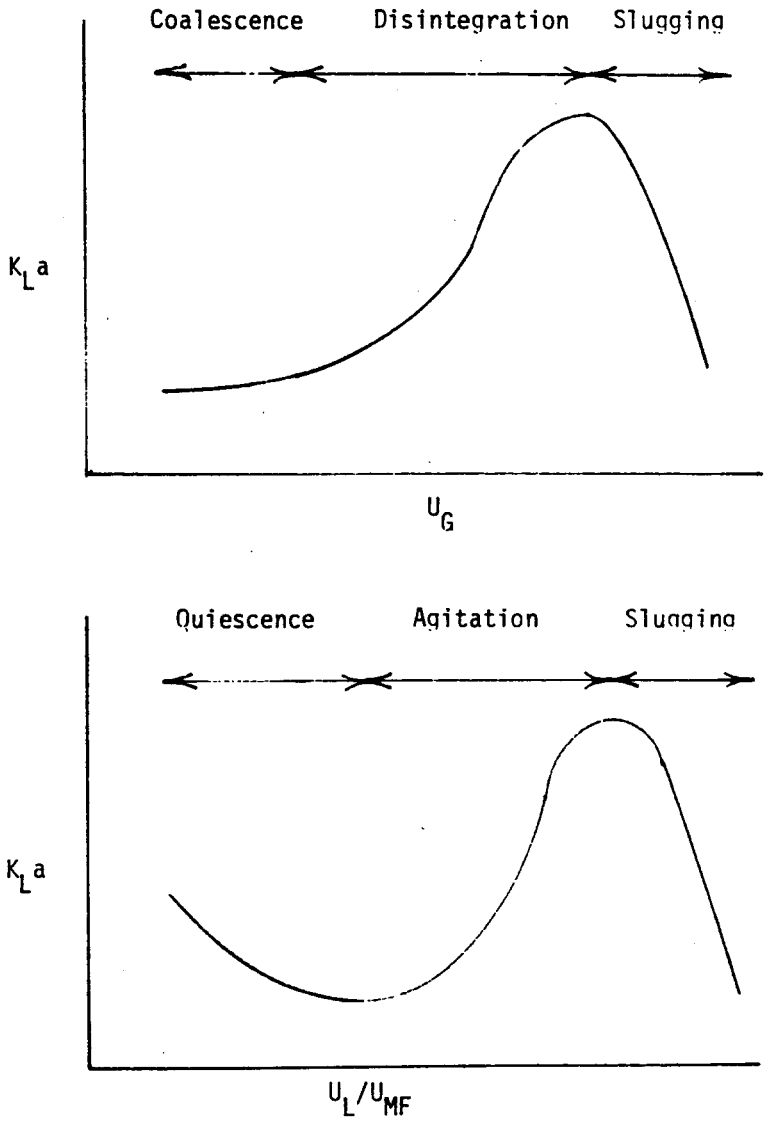

MASSACHUSETTS INSTITUTE OF TECHNOLOGY
SCHOOL OF CHEMICAL ENGINEERING PRACTICE
AT
OAK RIDGE NATIONAL LABORATORY

PROPOSED MASS TRANSFER MODELS

DATE	DRAWN BY	FILE NO.	FIG.
12-21-78	CBH	CEPS-X-283	8

A similar model can be proposed for K_La behavior with liquid velocity, as shown in Fig. 8b. At low U_L the liquid has little hydrodynamic effect, and transfer is determined by gas and particle characteristics. At moderate U_L, the liquid serves to transport the gas through the bed, reducing gas holdup without providing any significant agitation. This region is characterized by decreased transfer. At a U_L equal to 2.5 to 3 times the minimum fluidization velocity, substantial agitation increases the interfacial area and offsets this decrease in holdup, so that transfer is enhanced. This transfer increases until a point is reached where the buoyant force imparted to the particles reduces their inertia and aids in slugging.

Increasing particle diameters appear to shift the proposed models in Fig. 8 to the right. In regions of significant coalescence, the greater inertial effects of larger beads significantly support transfer. At increased velocities, this greater inertia causes more turbulence and hence larger interfacial area, which promotes transfer.

The decrease in K_La noted at high U_L/U_{MF} for the 6.0-mm bead diameter is a result of slugging caused by the higher minimum fluidization velocity associated with larger beads. A high liquid velocity is conducive to slugging as it reduces particle inertia and also aids in transporting the slugs through the column.

Mass transfer must clearly be inter-related with the changing hydrodynamics caused by variations of each parameter, so that a simple correlation of U_L, U_G, and d_p over a wide range of operating conditions is difficult to obtain. Bed operation, however, would occur within the region of bubble disintegration for which correlation has been obtained. Mass transfer was correlated by a quadratic function of liquid velocity, for which the quadratic constants were correlated as experimental functions of particle diameter and gas velocity. The resulting correlation is:

$$K_La = C_1\left(\frac{U_L}{U_{MF}}\right)^2 + C_2\left(\frac{U_L}{U_{MF}}\right) + C_3 \qquad (13)$$

where

$$C_1 = 9.1 \times 10^{-5}\, d_p^{1.70}\, U_G^{0.75}$$

$$C_2 = -4.5 \times 10^{-4}\, d_p^{1.58}\, U_G^{0.94}$$

$$C_3 = 1.75 \times 10^{-3}\, d_p^{1.24}\, U_G^{0.84}$$

The linear coefficients of determination for the constants are 0.91, 0.91, and 0.94, respectively, the overall coefficient of determination for the parabola being 0.83. A parity plot for the correlation, which uses the experimental data from Figs. 5 and 6, is presented in Fig. 9.

4.2 Comparison of Two- and Three-Phase $K_L a$'s

The effect of solid particles on the $K_L a$ depends on their size and density. Particles can have either a bubble-coalescing effect, which decreases interfacial area and reduces $K_L a$, or a bubble-disintegrating effect, which enhances interfacial area and increases $K_L a$ (11, 12). The observed effect depends on the relative importance of viscous and surface-tension forces of the gas-liquid phase to inertial particle forces. Viscous forces can be neglected as first approximation for dilute aqueous solutions, and the comparison is expressed in terms of the Weber number:

$$We_p = \frac{\rho_p U_R d_p}{\sigma_{GL}} \tag{14}$$

Systems with Weber numbers greater than three will be characterized by bubble disintegration and will otherwise be characterized by coalescence (13). For these experiments, Eq. (14) yields a critical particle diameter of about 2.5 mm, indicating that bubble-disintegration should predominate and thus mass transfer should be enhanced. The $K_L a$'s should then be higher than those for the corresponding two-phase system.

A comparison of three-phase and two-phase $K_L a$'s (see Appendix 8.3) reveals that generally the former are only slightly higher than the latter. However, both values are calculated using a superficial gas velocity based on the column cross-sectional area, when the use of local gas velocity is more appropriate. The local gas velocity is defined as:

$$U_{G,3\phi} = \frac{U_G}{\varepsilon_G} = \frac{U_G}{1 - \varepsilon_S - \varepsilon_L} \tag{15}$$

The ratio of local velocities in the two- and three-phase regions is:

$$\frac{U_{Gl,3\phi}}{U_{G,2\phi}} = \frac{(1 - \varepsilon_L)_{2\phi}}{(1 - \varepsilon_S - \varepsilon_L)_{3\phi}} \tag{16}$$

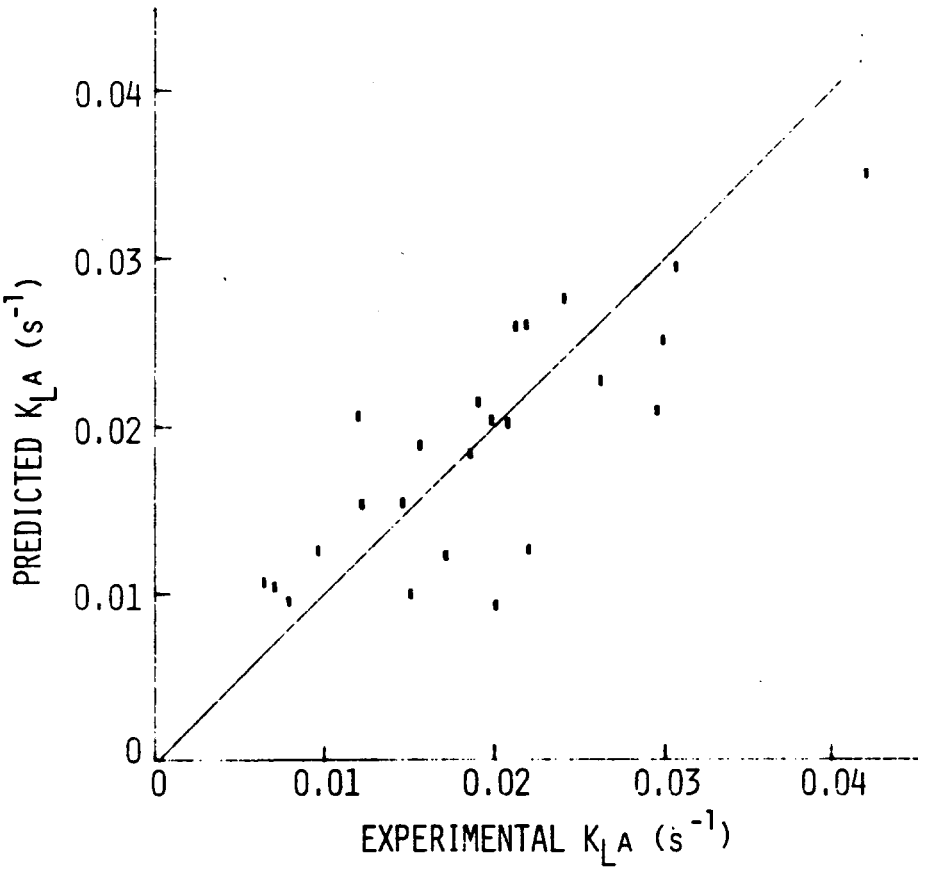

MASSACHUSETTS INSTITUTE OF TECHNOLOGY
SCHOOL OF CHEMICAL ENGINEERING PRACTICE
AT
OAK RIDGE NATIONAL LABORATORY

CORRELATION PARITY PLOT

DATE	DRAWN BY	FILE NO.	FIG.
12-21-72	NFS	283	9

Equation (16) can be approximated by

$$\frac{U_{G,3\phi}}{U_{G,2\phi}} = \frac{1}{1 - \varepsilon_{S,3\phi}} \tag{17}$$

For many experimental conditions, this is a fair approximation, and the three-phase K_La's based on local velocity, Eq. (17), are generally 2.5 times higher than those of the two-phase region (see Sect. 8.3).

4.3 Axial Dispersion Coefficient

Values for the axial dispersion coefficients were determined using Eq. (1), in which E_L and K_La appear simultaneously. Experimental K_La values were then combined with available liquid-phase O_2 concentration data (17), and E_L values were calculated using a technique described in Appendix 8.2.4.

In the thirty cases examined, the dispersion coefficient was found to be nearly zero, which indicates that liquid axial dispersion was negligible. Therefore, the liquid phase also exhibits plug flow at the experimental conditions investigated.

5. CONCLUSIONS

1. Dependence of K_La on U_L can be characterized by a three-region model: a low U_L region which exhibits decreased gas holdup and low transfer rates, a moderate U_L region which exhibits bubble disintegration and increased transfer rates, and a high U_L region which exhibits slugging and low transfer rates.

2. Within the bubble-disintegration region, K_La is correlated quadratically with U_L, and the constants are correlated exponentially with U_G and d_p.

3. K_La dependence on U_G can also be characterized by a three-region model: a low U_G region which exhibits bubble coalescence and low transfer rates, a moderate U_G region which exhibits bubble disintegration and increased transfer rate, and a high U_G region which exhibits slugging and low transfer.

4. Increased d_p promotes mass transfer at lower U_L and at all U_G.

5. For the operating conditions considered, the system was in plug-flow region for both gas and liquid phases.

6. RECOMMENDATIONS

1. The effect of bead diameter on hydrodynamic behavior should be further investigated.

2. $K_L a$ behavior at lower gas and liquid velocities should be investigated.

3. Experimentation with repeated runs should be undertaken to statistically confirm the sampling method.

4. The sampling taps should be redesigned to minimize gas/liquid interaction within the lines.

7. ACKNOWLEDGMENTS

The authors thank their consultants, J.M. Begovich, S.D. Clinton, and J.S. Watson for their advice and encouragement. Assistance in data analysis by C.L. Begovich was appreciated. Special thanks are due to J.D. Hewitt for technical assistance.

8. APPENDIX

8.1 Gas Sampling System

Gas-phase samples were taken from the bed through a probe inserted into the center of the bed through a port in the column wall (see Fig. 10). The probe was constructed of Teflon tubing, slit longitudinally at the bottom to admit gas bubbles while excluding glass beads. The probe was connected to a glass tee, from which the liquid flowed downward and was recycled. The flow rate was adjusted so that a liquid head was maintained below the tee to force the gas phase upwards to the sample chamber.

The monitoring system consisted of two Instrument Lab. O_2 electrodes and amplifiers, a dual-pen chart recorder and two-variable potentiometers, which served as voltage supplies. The amplifiers provided outputs of 0-100 mV, which were linear with respect to the partial pressure of oxygen at the electrode. They were calibrated to provide an output of 100 mV for air. In the experiments the concentration of O_2 in the gas phase was reduced by about 8%. The potentiometers applied a bias voltage of 90 mV to the chart recorder to permit examination of O_2 concentrations over an expanded scale.

8.2 Sample Calculations

8.2.1 Henry's Constant

Henry's constant, m, is defined in this report as the ratio of liquid concentration to gas concentration at equilibrium, i.e.,

$$m = \frac{C_{L,i}}{C_{G,i}} \tag{18}$$

$m = 5.76 \times 10^{-2}$ for O_2-water at 1 atm and is linear with respect to pressure (12). Therefore,

$$m = \frac{p}{1\ atm} \times 5.76 \times 10^{-2} \tag{19}$$

where p is the pressure for the region of interest.

The sample calculation is presented for Run 5 during which gas was sampled from ports 4 and 7. To determine the K_La for the three-phase region, p was closely approximated as the arithmetic average pressure of the region between taps 4 and 7. The pressure at a given tap p_j was given by:

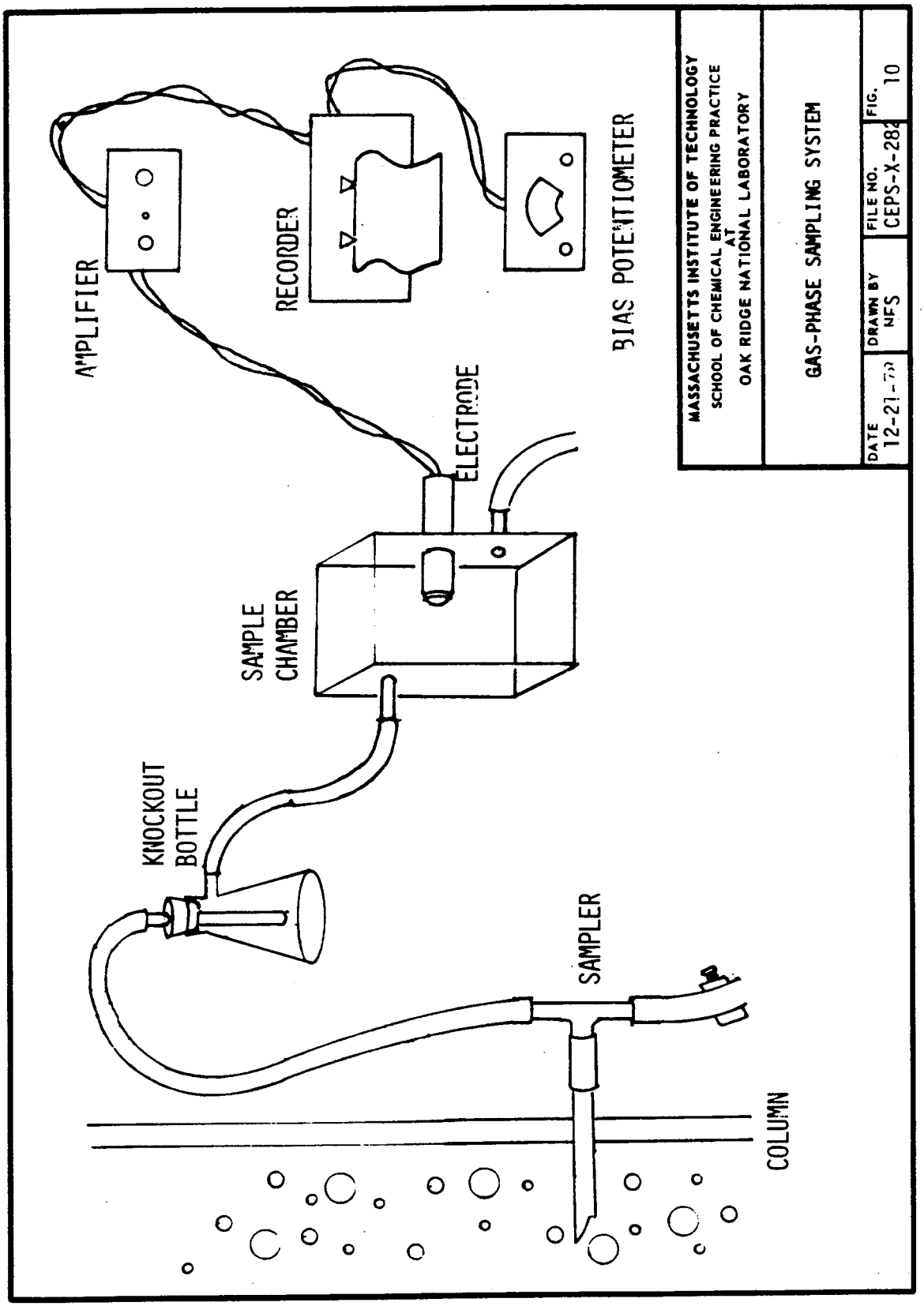
AMPLIFIER
RECORDER
BIAS POTENTIOMETER
ELECTRODE
SAMPLE CHAMBER
KNOCKOUT BOTTLE
SAMPLER
COLUMN
MASSACHUSETTS INSTITUTE OF TECHNOLOGY
SCHOOL OF CHEMICAL ENGINEERING PRACTICE
AT
OAK RIDGE NATIONAL LABORATORY
GAS-PHASE SAMPLING SYSTEM
DATE 12-21-7?
DRAWN BY NFS
FILE NO. CEPS-X-284
FIG. 10

$$p_j = p_b + p_m - \Delta p_j \tag{20}$$

p_b and p_m were 0.980 and 0.171 atm respectively for this run and were read from the manometers. Δp_j (atm) was determined from:

$$\Delta p_j = \frac{[(W_B - W_j) - (W_{B,o} - W_{j,o}) + \Delta h]}{1000} \tag{21}$$

W_B and $W_{B,o}$ were 56.5 and 46.7 cm H_2O, respectively. For tap 4, W_j, $W_{j,o}$ and Δh were 43.2, 45.2, and 24.0 cm H_2O. For tap 7, the corresponding values were 28.7, 39.6, and 48.0 cm H_2O. Using Eq. (21), Δp_4 is 0.035 atm, and Δp_7 is 0.070 atm. Then from Eq. (20),

$$p_4 = 0.980 + 0.171 - 0.035 = 1.116 \text{ atm}$$

and

$$p_7 = 0.980 + 0.171 - 0.070 = 1.081 \text{ atm}$$

The average pressure between taps 4 and 7 is 1.099 atm, which gives an m-value of 6.3×10^{-2} from Eq. (19).

8.2.2 Solid-Phase Volume Fraction

The solid-phase volume fractions of the three-phase and transition regions are defined as:

$$\varepsilon_{S,3\phi} = \frac{V_{p,3\phi}}{V_{3\phi}} \tag{22a}$$

$$\varepsilon_{S,t} = \frac{V_{p,t}}{V_t} \tag{22b}$$

where

$$V_{p,3\phi} + V_{p,t} = V_p \tag{23}$$

The total particle mass was known, and V_p was evaluated by a density calculation using data from (1). For run 5, V_p was 1482 cm^3. The heights of the three-phase and transition regions were determined within 2% error by three independent observations and were used to calculate volumes of these regions. $V_{3\phi}$ and V_t were 2370 and 365 cm^3, respectively.

The axial solids holdup profile in the transition region is closely approximated by the error function (1). This behavior indicates that it is reasonable to model the average solid void fraction in this region by:

$$\varepsilon_{S,t} = \frac{1}{2}\,\varepsilon_{S,3\phi} \tag{24}$$

Equations (22) through (24) were solved simultaneously for the four unknowns ($\varepsilon_{S,3\phi}$, $\varepsilon_{S,t}$, $V_{p,3\phi}$, and $V_{p,t}$). This yielded values for $V_{p,3\phi}$ and $\varepsilon_{s,3\phi}$ of 1376 cm^3 and 0.58, respectively.

8.2.3 Mass Transfer Coefficient

Equation (7) may be rearranged:

$$\frac{dC_G}{C_G} = -\frac{K_L a\, m\, dh}{U_G} \tag{25}$$

If $C_G(h_1) = C_{G_1}$, $C_G(h_2) = C_{G_2}$, and $K_L a$ and m are assumed constant, integration of Eq. (25) gives, when rearranged:

$$K_L a = \frac{U_G \ln\left(\frac{X_1}{X_2}\right)}{m\,\Delta h} \tag{26}$$

For Run 5, m is 6.3×10^{-2}, U_G is 8.68 cm/s, Δh is 24 cm, X_1 is 98.02, and X_2 is 97.68. Substituting into Eq. (26) yields $K_L a = 0.0199\ s^{-1}$.

8.2.4 Dispersion Coefficient

The solution to Eq. (1) is given by Hartland and Mecklenburgh (7):

$$\frac{mC_{G_e} - C_L}{mC_{G_e} - C_{L_e}} = X = 1 - \left(\frac{1}{F+1}\right)\left[\frac{\left(1 - \frac{\alpha_1 E_L}{U_L H}\right) - e^{\alpha_1 z}}{\alpha_1 e^{\alpha_1}} - \frac{\left(1 - \frac{\alpha_2 E_L}{U_L H}\right) - e^{\alpha_2 z}}{\alpha_2 e^{\alpha_2}}}{\frac{1 - \frac{\alpha_1 E_L}{U_L H}}{\alpha_1 e^{\alpha_1}} - \frac{1 - \frac{\alpha_2 E_L}{U_L H}}{\alpha_2 e^{\alpha_2}}}\right] \tag{27}$$

where

$$F = \frac{mU_L}{U_G} \tag{28}$$

and

$$\alpha_1, \alpha_2 = \alpha_+, \alpha_- = \frac{-[(\frac{E_L}{U_L^2})(K_L a) - (\frac{1}{F})] \pm \sqrt{[(\frac{E_L}{U_L^2})(K_L a) - (\frac{1}{F})]^2 + (4)(\frac{1}{F})(\frac{E_L}{U_L^2})(K_L a)(\frac{1}{F}+1)}}{(2)(\frac{1}{F})(\frac{E_L}{U_L H})} \tag{29}$$

For a given $K_L a$, E_L can be calculated iteratively.

For Wu's Run 16 (17), m was 0.0628, U_G was 4.63 cm/s, U_L was 3.25 cm/s, and h was 32 cm. Also, $mC_{G_i} - C_{L_1} / mC_{G_i} - C_{L_2} = 0.93$. From Run 2, $K_L a$ was 0.0071. At $E_L = 0.001$, $mC_{G_i} - C_{L_1} / mC_{G_i} - C_{L_2} = 0.933$.

8.2.5 Error Analysis

The uncertainty of the calculated mass transfer coefficients was determined using an expression derived by Kline and McClintock (10) for single sample experiments. If Q is a function of n independent variables,

$$Q = f(q_1, q_2, \ldots, q_n) \tag{30}$$

The uncertainty associated with Q is given by:

$$\Delta Q = \left[\sum_{i=1}^{N} (\frac{\partial f}{\partial q_i} \Delta q_i)^2 \right]^{1/2} \tag{31}$$

where Δq_i is the uncertainty associated with each of the independent variables.

Equation (12) relates $K_L a$ to measurable quantities and was used to determine error bounds for all experimental runs.

$$K_L a = \frac{U_G \ln(\frac{X_e}{X_\ell})}{m\Delta h} \qquad (12)$$

Table 2 presents the estimated uncertainties of each independent variable and sample experimental values from one run.

Table 2. Error Data from Run 24

q_i	U_G (cm/s)	Δh (cm)	m	X_e (%)	X_o (%)
Experimental Value	12.81	24	0.0653	97.34	96.84
Δq_i	0.15	0.5	6.2×10^{-4}	0.05	0.05
$(\frac{\partial K_L a}{\partial q_i} \Delta q_i)^2$	2.43×10^{-7}	7.69×10^{-7}	1.61×10^{-7}	1.76×10^{-5}	1.78×10^{-5}

$\Delta K_L a$ was calculated to be 0.0061 s^{-1} based on Table 2. The tabulation indicates that O_2 measurements contributed 95% of this value. The error was linear with gas velocity and constant for a given gas velocity, the values being 0.0021, 0.0041, and 0.0061 s^{-1} for gas velocities of 4.3, 8.7, and 12.9 cm/s, respectively.

8.3 Summary of Experimental Results

d_p = 3.2 mm

Run No.	U_L (cm/s)	U_L/M_{MF}	U_G (cm/s)	$K_L a_{2\phi}$ (s^{-1})	$K_L a_{3\phi}$ (s^{-1})	$1 - \epsilon_{s,3\phi}$
1	2.03	1.64	4.35	0.0137	0.0172	0.63
2	2.70	2.17	4.35	0.0102	0.0071	0.62
3	4.04	3.26	4.35	0.0103	0.0151	0.56
4	6.74	5.43	4.35	0.0074	0.0263	0.47
5	1.47	1.54	8.68	0.0082	0.0199	0.58

Run No.	U_L (cm/s)	U_L/M_{MF}	U_G (cm/s)	$K_La_{2\phi}$ (s^{-1})	$K_La_{3\phi}$ (s^{-1})	$1 - \varepsilon_{S,3\phi}$
6	1.96	2.06	8.68	0.0145	0.0123	0.56
7	2.93	3.09	8.68	0.0108	0.0065	0.53
8	4.77	5.02	8.60	0.0183	0.0121	0.47
9	1.28	1.54	12.46	0.0211	0.0219	0.49
10	1.69	2.04	12.95	0.0083	0.0184	0.49
11	2.54	3.06	12.90	0.0136	0.0078	0.47
12	4.24	5.10	12.90	0.0148	0.0207	0.45
d_p = 4.6 mm						
14a	9.60	4.62	4.30	0.0438	0.0213	0.65
14b	7.48	4.68	8.57	0.0436	0.0240	0.56
15	6.23	4.65	12.80	0.517	0.0295	0.53
16	2.92	1.41	4.28	0.0125	0.0157	0.38
17	5.85	2.81	4.28	0.0180	0.0097	0.51
18	3.90	1.87	4.28	0.0112	0.0146	0.42
19	4.47	2.80	8.54	0.0162	0.0220	0.47
20	2.98	1.86	8.55	0.0182	0.0192	0.41
21	2.24	1.40	8.55	0.0221	0.0305	0.39
22	3.72	2.78	12.79	0.0170	0.0201	0.49
23	2.48	1.85	12.86	0.0060	0.0299	0.43
24	1.86	1.39	12.81	0.0209	0.0421	0.41
d_p = 6.0 mm						
31	4.04	1.43	4.34	0.0226	0.0145	0.45
32	5.39	1.91	4.37	0.0308	0.0206	0.49
33	8.09	2.87	4.34	0.0173	0.0263	0.58
34	11.2	3.98	4.34	0.0179	0.0351	0.58
35	3.12	1.45	8.67	0.0251	0.0187	0.44
36	4.16	1.93	8.67	0.0213	0.0088	0.47
37	6.25	2.89	8.70	0.0280	0.0160	0.52
38	10.4	4.82	8.67	0.0118	0.0198	0.65
39	2.78	1.46	12.98	0.0332	0.0270	0.44
40	3.70	1.94	12.98	0.0172	0.0148	0.49

Run No.	U_L (cm/s)	U_L/M_{MF}	U_G (cm/s)	$K_L a_{2\phi}$ (s^{-1})	$K_L a_{3\phi}$ (s^{-1})	$1 - \varepsilon_{S,3\phi}$
41	5.55	2.90	12.95	0.0248	0.0268	0.53
42	9.25	4.84	12.86	0.0408	-	-
43	4.04	1.43	4.32	-	0.0115	0.45
44	3.12	1.45	8.59	-	0.0174	0.44
45	9.25	4.84	12.80	-	0.0084	0.61
46	8.09	2.87	4.32	-	0.0246	0.58
47	5.39	1.91	4.32	-	0.0197	0.49
48	4.16	1.93	8.62	-	0.0193	0.47
49	6.25	2.89	8.61	-	0.0158	0.52
50	5.55	2.90	12.87	-	0.0189	0.53
51	2.78	1.46	12.90	-	0.0226	0.44
52	3.70	1.94	12.90	-	0.0251	0.49

8.4 Nomenclature

A concentration of solute gas reactant

B concentration of liquid phase reactant

C concentration, gmole/cm^3

d_p particle diameter, mm, cm

D bed diameter, cm

D_G diffusivity of gas in liquid phase, cm/s

E dispersion coefficient, cm^2/s

h height, cm

H column height, cm

$K_C a$ overall mass transfer coefficient, s^{-1}

$K_G a$ gas-side mass transfer coefficient, s^{-1}

$K_L a$ liquid-side mass transfer coefficient, s^{-1}

K_{mn} generalized rate constant of reaction A + B → product